Colloids and Surfaces B: Biointerfaces 161 (2018) 654–661

Contents lists available at ScienceDirect

Colloids and Surfaces B: Biointerfaces

journal homepage: www.elsevier.com/locate/colsurfb

Full length article

Soybean peroxidase immobilized onto silica-coated superparamagnetic iron oxide nanoparticles: Effect of silica layer on the enzymatic activity

Jorge A. Donadelli[a], Fernando S. García Einschlag[a], Enzo Laurenti[b], Giuliana Magnacca[b,c], Luciano Carlos[d,*]

[a] Instituto de Investigaciones Fisicoquímicas Teóricas y Aplicadas (INIFTA), CCT-La Plata-CONICET, Universidad Nacional de La Plata, Diag 113 y 64, La Plata, Argentina
[b] University of Torino, Department of Chemistry, Via P. Giuria 7, 10125, Torino, Italy
[c] NIS Interdepartmental Centre, Via P. Giuria 7, 10125, Torino, Italy
[d] Instituto de Investigación y Desarrollo en Ingeniería de Procesos, Biotecnología y Energías Alternativas, PROBIEN (CONICET-UNCo), Buenos Aires, 1400, Neuquén, Argentina

ARTICLE INFO

Article history:
Received 15 September 2017
Received in revised form 9 November 2017
Accepted 16 November 2017

Keywords:
Peroxidase
Magnetic nanoparticles
Biocatalysts
Wastewater treatment

ABSTRACT

Peroxidase immobilization onto magnetic supports is considered an innovative strategy for the development of technologies that involves enzymes in wastewater treatment. In this work, magnetic biocatalysts were prepared by immobilization of soybean peroxidase (SBP) onto different silica-coated superparamagnetic iron oxide nanoparticles. The obtained magnetic biocatalysts were tested for the degradation of malachite green (MG), a pollutant often found in industrial wastewaters and with significant drawbacks for the human and environmental health. A deep physicochemical characterization of the materials was performed by means of X-ray diffraction (XRD), Fourier Transform Infrared Spectroscopy (FTIR), High Resolution-Transmission Electron Microscope (HR-TEM) and magnetization measurements among others techniques. Results showed high immobilization yield of SBP onto nanomaterials with excellent properties for magnetic recoverability. A partial loss of activity with respect to free SBP was observed, compatible with the modification of the conformational structure of the enzyme after immobilization. The structural modification depended on the amount (and thickness) of silica present in the hybrid materials and the activity yield of 43% was obtained for the best biocatalyst. Thermal stability and reusability capacity were also evaluated.

1. Introduction

Peroxidases are able to catalyse the oxidation of a large variety of aromatic compounds by hydrogen peroxide over a wide range of pH, temperature and ionic strength [1,2]. These features set up a great potential for the use of peroxidases in the decontamination of wastewater containing aromatic compounds that are refractory to conventional treatments. In the last years, soybean peroxidase (SBP) has received much attention because it could be easily obtained in large amount, has a high thermal stability and is more resistant to deactivation than other peroxidases [3,4]. SBP is a class III secretory plant peroxidase characterized by a Fe(III)-heme protoporphyrin IX prosthetic group as active site [5]. The catalytic cycle of plant heme peroxidases involves the two-electron reduction of hydrogen peroxide and the one-electron oxidation of two substrate molecules via the well characterized intermediates Compound I and Compound II [6]. Such mechanism allows the oxidation of several inorganic and organic substrates in a broad range of pH with a maximum activity at pH 5 – 6. Recently, Steevensz et al. [3] successfully applied crude SBP to treat alkyd resin wastewater at pilot scale reaching almost total phenol depletion. The main drawbacks of using soluble enzymes in wastewater treatment are the relatively high extraction cost, difficulties in reuse and enzyme short catalytic lifetime due to the inactivation induced by the polymerization process [7]. Enzyme immobilization was demonstrated

* Corresponding author at: Instituto de Investigación y Desarrollo en Ingeniería de Procesos, Biotecnología y Energías Alternativas, PROBIEN (CONICET-UNCo), Buenos Aires, 1400, Neuquén, Argentina.
E-mail address: luciano.carlos@probien.gob.ar (L. Carlos).

https://doi.org/10.1016/j.colsurfb.2017.11.043
0927-7765/

as an effective approach to overcome these limitations, since the supported enzyme can be recovered at the end of the treatment and reused. Moreover, it has been reported that immobilization can increase thermal resistance and activity in organic solvents [8]. Therefore, an efficient immobilization of enzymes on solid supports should ensure enzyme stability in terms of activity, recoverability of the biocatalyst and allow free diffusion of substrates and reaction products. Various strategies for the enzyme immobilization are reported, including mainly physical adsorption and covalent attachment [9,10]. Comparatively, covalent immobilization can eliminate or significantly reduce leaching of peroxidase and can increase stability [11]. Typical biocatalyst supports include polymers, silica, alumina, titania, and other metal oxides that can be separated by conventional separation techniques such as filtration and centrifugation [12–15]. Magnetic nanoparticles (MNPs) have gained considerable attention as biocatalyst supports because of their response to an applied magnetic field. Magnetic separation has emerged as a robust, highly efficient and rapid catalyst separation tool with many advantages compared to biocatalyst isolation by filtration or centrifugation [16]. Magnetic iron oxides such as magnetite (Fe_3O_4) and maghemite (γ-Fe_2O_3) are promising candidates for enzyme immobilization as they offer high specific areas, low cost preparation, facility of reuse and high enzyme loading capability [17]. However, magnetic iron oxides nanoparticles are susceptible to air oxidation and are easily aggregated in aqueous systems [11,18]. Therefore, for the application of these nanoparticles as biocatalyst supports, the stabilization of the iron oxide nanoparticles by surface modification is needed. Since the immobilized enzyme onto magnetic nanoparticles has reported some disadvantages, including lowered activity, conformational change of the enzyme and mass transfer limitations [7], controlling the key parameters in the enzymatic immobilization are critical for the design of magnetically recoverable biocatalysts. Several works reported different methods for the immobilization of a variety of enzymes, such as horseradish peroxidase, laccase, urease and serum albumin, onto magnetic supports [11,17,19–21]. However, to the best of our knowledge, only one recent paper studied the immobilization of SBP on magnetic nanoparticles, reaching higher enzymatic activities than free SBP [7].

In the present work we investigated the covalent immobilization of SBP onto different modified magnetic nanoparticles at low enzyme concentration using silica as surface coating to protect magnetic iron oxide core and a functionalized outer coating with (3-aminopropyl) triethoxysilane (APTES). In particular, the effect of the surface coating agents on both the SBP immobilization yield and the enzymatic activity was analyzed. The resulting biocatalysts were characterized by means of several experimental techniques, including FTIR spectroscopy, HR-TEM, XRD, gas-volumetric adsorption of N_2 at 77 K and magnetization curves. Finally, the activity and stability properties of immobilized SBP were tested toward the removal of Malachite Green (MG) from aqueous solution. MG, a triarylmethane dye that can cause mutagenic and carcinogenic effects [22], is an effective antimicrobial and antifungal agent in food industry and very used for dyeing wool, silk, cotton, leather, etc. [23].

2. Materials and methods

2.1. Reagents

Soybean peroxidase (SBP, EC 1.11.1.7) RZ = 2.0 was purchased from Bio-Research Products Inc. (activity 1269 U/mg, lot# SBP-B275P154); glutaraldehyde (25%), tetraethylorthosilicate (TEOS, 98%), 3-aminopropyltriethoxysilane (APTES, 98%), NH_4OH (33%) and $FeCl_3$ (97%) from Sigma-Aldrich, ethanol (99.8%) and $FeSO_4.7H_2O$ (99.5%) from Fluka; Malachite Green from Anedra and H_2O_2 (30%) from Cicarelli. All chemicals were used without further purification.

2.2. Preparation of magnetic materials

2.2.1. Synthesis of magnetic iron oxide nanoparticles (MNP)

Iron oxide nanoparticles were prepared by co-precipitation method [9] in nitrogen atmosphere using 5.13 g of $FeCl_3$ and 2.67 g of $FeSO_4{\cdot}7H_2O$ solubilised in 100 mL of water. The solution, constantly kept under stirring, was heated at 90 °C and then 10 mL of NH_4OH 30% and 50 mL of water were added. The reaction was kept occurring for 30 min, after that the solution was cooled down at RT and the black solid product was magnetically separated from the supernatant using a magnet. The solid was washed with deionised water four times, dried in a rotavapor at 80 °C and subsequently stored under N_2 until use for the syntheses of the different composite materials.

2.2.2. Functionalization of MNP with APTES (NPA)

MNP were functionalized with APTES by a modification of the Keziban procedure [11]. 3.0 g MNP were dispersed in 150 mL of ethanol/water (1:1) solution. The suspension was kept under nitrogen and sonicated for 10 min, after that 11.12 mL of APTES were added and the mixture was stirred for 2 h at 40 °C. The material obtained (NPA) was washed three times with ethanol/water solution and dried in rotavapor at 80 °C.

2.2.3. Synthesis of silica coated MNP with APTES surface modification (NPTAI and NPTAII)

MNP were coated with silica by sequential reactions with TEOS and APTES [9]. In brief, 2 gr of MNP were dispersed in 400 mL of ethanol and sonicated for 10 min. TEOS (2 or 5.5 mL), NH_4OH (30 mL) and H_2O (60 mL) were added and the mixture was kept under stirring for 5 h. After the reaction, the solid was washed with ethanol/water solution and dried in rotavapor at 80 °C. Successively, 2 g of these materials were suspended in ethanol, sonicated for 10 min, and 60 mL of APTES were added during stirring and kept reacting for 2 h at 25 °C and 2 h at 50 °C. Finally, the samples were washed for three times in ethanol/water and dried in rotavapor at 80 °C. The samples prepared with 2 and 5.5 mL of TEOS were named NPTAI and NPTAII, respectively.

2.2.4. SBP immobilization

SBP was immobilized onto the surface of the synthesized materials using glutaraldehyde as spacer [14] (Fig. 1). 1 g of MNP, NPA, NPTAI or NPTAII was introduced in a 100 mL solution of glutaraldehyde (2.5%) in phosphate buffer (0.1 M at pH 7). The mixture was stirred for 1 h in the dark and the products were magnetically separated and washed with the buffer solution twice. Then, each material was incubated with 40 mL of SBP solution 4.96×10^{-6} M in phosphate buffer for 15 h at 4 °C and continuous stirring. Quantification of SBP immobilized was determined from the difference of absorption at 403 nm ($\varepsilon_{SBP,403nm} = 96400\ M^{-1}cm^{-1}$ [24]) in the supernatant solution before and after the contact of SBP with the nanomaterials. All the obtained solids were washed with 4 mL of phosphate buffer solution twice. Possible release of SBP from the nanomaterial to the aqueous media during the washing process was monitored by UV–vis spectroscopy. In all cases, no absorption at 403 nm was detected in the washing solution, indicating no release of SBP. Depending on the nanomaterial used for the enzyme immobilization (MNP, NPA, NPTAI and NPTAII), the SBP containing materials were named MNP-SBP, NPA-SBP, NPTAI-SBP and NPTAII-SBP, respectively.

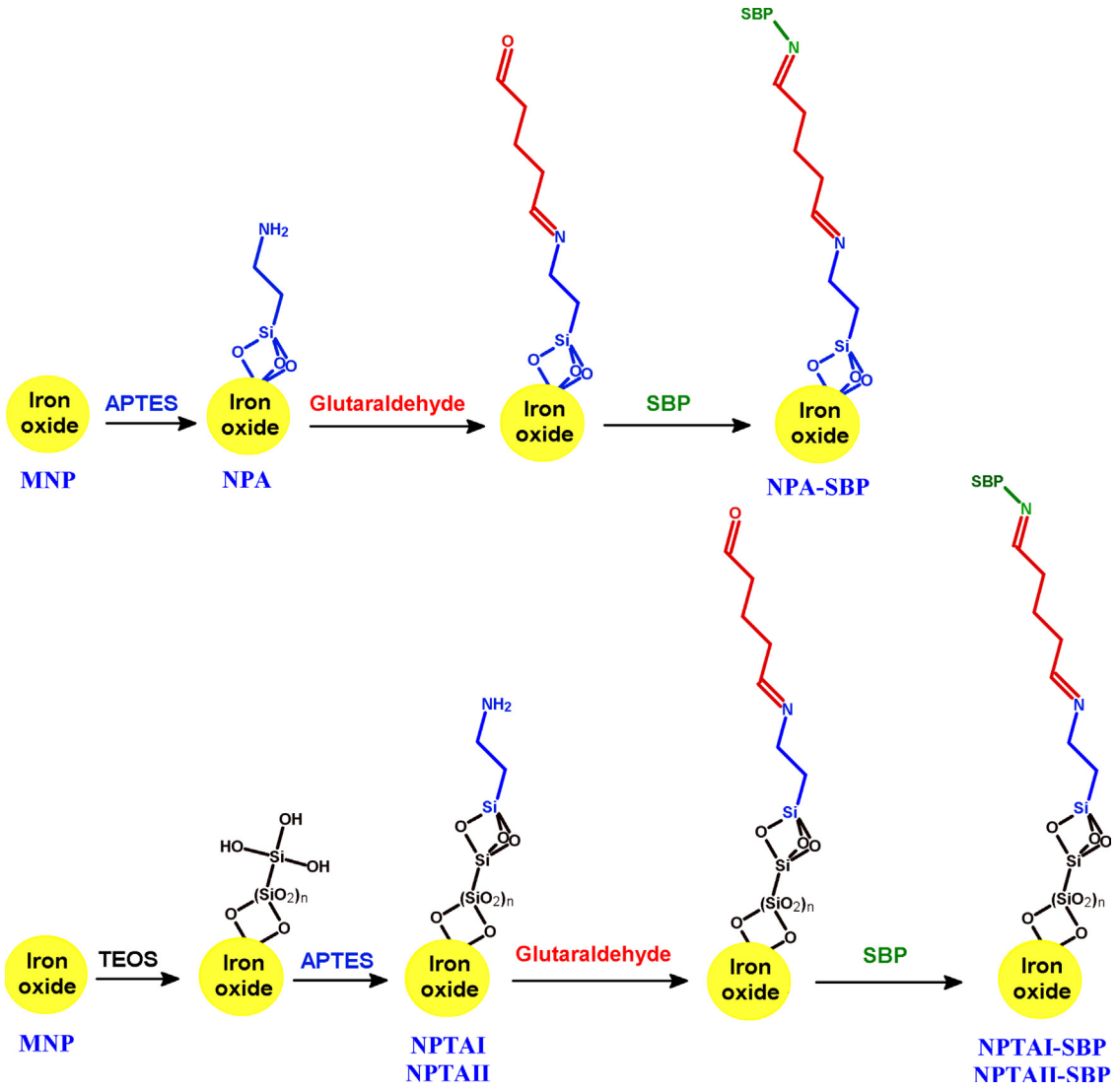

Fig. 1. Synthesis scheme for the immobilization of SBP on magnetic nanomaterials.

2.2.5. Physicochemical characterization

Specific surface area and porosity of materials were measured by means of N_2 adsorption at 77 K with ASAP2010 instrument by Micromeritics applying BET method and BJH to the adsorption branch of the isotherms, respectively. All the materials were outgassed at room temperature for 12 h (residual pressure 10^{-2} mbar) before adsorption experiments in order to remove atmospheric contaminants from surface and pores. HR-TEM images were recorder with a JEOL 3010-UHR instrument (acceleration potential: 300 kV). Samples for TEM investigation were supported onto holed carbon coated copper grid by dry deposition. XRD data were obtained with a diffractometer PW3040/60 X'Pert PRO MPD (PANalytical) using a Cu source and working with Bragg-Brentano geometry. The software MAUD was used for Rietveld refinement of diffractograms. FTIR spectra were obtained by means of IFS28 instrument by Bruker, in the range 4,000–400 cm^{-1} with 128 scans and a resolution of 4 cm^{-1}. The spectra were recorder on samples dispersed in KBr powder (ratio material/KBr = 1:30) and pressed to form pellets. ζ-potential values were obtained on a Litesizer ™500 Anton Paar. Magnetization curves were obtained with a LakeShore 7404 vibrating sample magnetometer. The hysteresis loop of the samples was registered at room temperature as the magnetic field was cycled between −20,000 and 20,000 G.

2.2.6. MG degradation

Malachite Green (MG) was selected as model pollutant to test the enzymatic activity of the prepared nanomaterials. MG concentration was determined using a UV–vis Cary-60 spectrophotometer. In a typical biocatalytic test, 0.01 g of material was incubated with 5 mL of MG solution (0.08 mM) in acetate buffer (0.1 M) at pH 5.5 for 60 min under magnetic stirring at the desired temperature. Then, hydrogen peroxide ($[H_2O_2]_0/[MG]_0 = 10$) was added to the reaction mixture and samples were withdrawn at different reaction times. The samples supernatant were magnetically separated, filtered with a 0.45 μm cellulose acetate filter and analyzed by UV–vis spectroscopy at 614 nm. The effect of the reaction temperature on the activity of the biocatalysts was studied in the range 25–95 °C. The reusability of biocatalyst was investigated by successive MG degradation tests conducted under the same reaction conditions described above. After the completion of the reaction, in the first cycle, the supported-SBP was magnetically recovered from the reaction solution, washed with buffer solution and placed again in contact with new solution of MG and H_2O_2 for the next degradation cycle. The residual activity of the biocatalyst was measured up to 10 recovery cycles. Control MG degradation experiments were performed using free SBP at the concentration of 9.02×10^{-9} M. In order to obtain the optimal H_2O_2 concentration

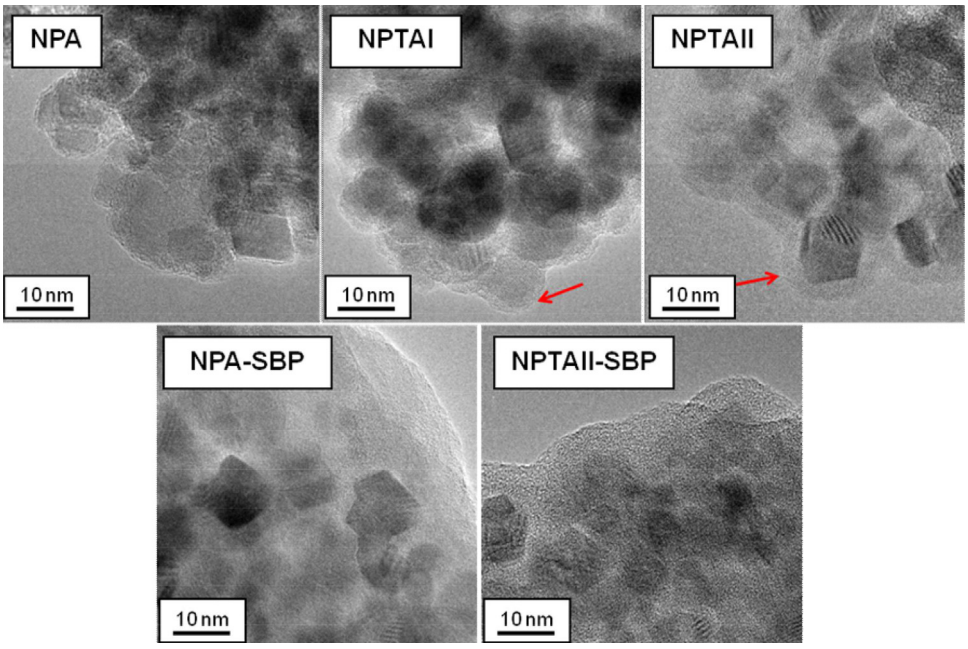

Fig. 2. Upper section: HRTEM images of biocatalyst (from left to right NPA, NPTAI and NPTAII). The arrows evidence the presence of the amorphous (siliceous) layer around crystalline particles. Lower section: HRTEM images of biocatalysts NPA-SBP and NPTAII-SBP.

Table 1
Results related to the immobilization of SBP on different supports.

Samples	% SBP immobilised	gr SBP/gr NP
MNP-SBP	Not detected	–
NPA-SBP	89.5	0.16
NPTAI-SBP	98.0	0.18
NPTAII-SBP	74.3	0.14

for the degradation of MG with free SBP, the effect of H_2O_2 concentration was also studied at different $[H_2O_2]/[MG]$ ratios: 0.5, 1, 3, 10 and 30.

3. Results and discussion

3.1. Characterization of nanomaterials

The results of the enzyme immobilization onto each nanomaterial (Table 1) showed high yields, except for NP-SBP where no SBP was bonded to the material surface. Saidman et al. [25] reported that the direct immobilization of horseradish peroxidase onto magnetite could be successfully achieved by glutaraldehyde activation in more severe conditions (e.g. 3.5 h at 80 °C). However, according to our data, the presence of $-NH_2$ functional group on the nanomaterial surface seems to play a fundamental role for the SBP immobilization in our experimental conditions (i.e. 1 h at room temperature). The absence of SBP in the solutions used for washing the materials after SBP immobilization procedure indicates that the enzyme is strongly bonded to the magnetic materials. The physicochemical characterization was performed only on the systems where SBP was actually immobilized.

Fig. 2 reports the HR-TEM images obtained for NPA, NPTAI and NPTAII, and for SBP-NPA and SBP-NPTAII. In general, for all samples, aggregates of particles roughly spherical, hexagonal and cubic in shape, with a crystalline core are observed. The crystalline particle size analysis evidenced a quite narrow size distribution centred at 10 nm in all cases (Figs. S1, Supplementary data). The lattice fringe patterns are associated with (210) (221) (310) (320) (321) diffraction planes of maghemite (γ-Fe_2O_3) (card# 00-039-1346, ICCD database). Although these planes are not assignable to magnetite (Fe_3O_4) phases, the presence of Fe_3O_4 cannot be excluded. Moreover, an amorphous silica shell covering entirely the crystalline nanoparticles with an average thickness of 1–2 and 4–5 nm for NPTAI and NPTAII, respectively, can be observed. This increment of the silica thickness observed for NPTAII reflects the higher TEOS concentration used in the synthesis process. The crystalline particles observed after the immobilization process maintain their original behaviours.

Fig. S2, in the Supplementary data, shows the XRD patterns for MNP, NPA-SBP, NPTAI-SBP and NPTAII-SBP. The position of the peaks for all materials are coincident with those of the γ-Fe_2O_3 and Fe_3O_4 phases, detail signals are present at $2\theta = 18.3°$, 30.2°, 35.6°, 43.3°, 53.8°, 57.3°, 62.9° and 90.2° associated to (111), (220), (311), (400), (422), (511), (440) and (731) planes of the two mentioned oxides. This confirms that the functionalisation process of the MNP surface with APTES and TEOS did not modify the original crystalline organisation. The presence of a peak at around $2\theta = 32°$ is due to synthesis by-products (ammonium salts), remaining after the washing process. The average size of the iron oxide crystalline domains obtained by applying Rietveld refinement were 15.7, 19.4, 12.0 and 16.6 nm for MNP, NPA, NPTAI and NPTAII, respectively. These values are slightly higher than those directly measured by HR-TEM.

FTIR spectra obtained from NPA, NPTAI and NPTAII are shown in Fig. S3 of the Supplementary data. The band at 578 cm^{-1} with a shoulder at 630 cm^{-1} is associated with Fe–O vibrations [26]. The reaction of APTES at the surface of NPA was confirmed by the bands at 996 and 1113 cm^{-1} assigned to the asymmetric vibration of Si–OH and Si-O groups, respectively [27]. For both NPTAI and NPTAII a broad band at 1070–1100 cm^{-1} and a peak at 800 cm^{-1} attributed to asymmetric and symmetric vibration Si-O-Si, respectively, revealed the presence of silica in these materials [27] and a more intense signal observed in NPTAII sample corroborates the hypothesis that a larger amount of silica was formed on this sample. The band at 1623 cm^{-1}, observed for all samples, can be referred to the NH_2 bending mode of free NH_2 group [11], confirming the presence of terminal amino groups at the surface of the biocatalyst support. The FTIR spectra obtained after the incubation of the

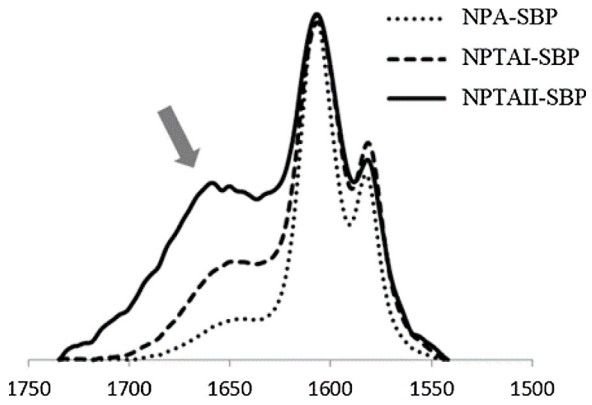

Fig. 3. FTIR spectra of NPA, NPTAI and NPTAII in the amide I and II signal range normalized at 1604 cm^{-1} band intensity. The grey arrow indicates the position expected for Amide I signal related to α-helix configuration.

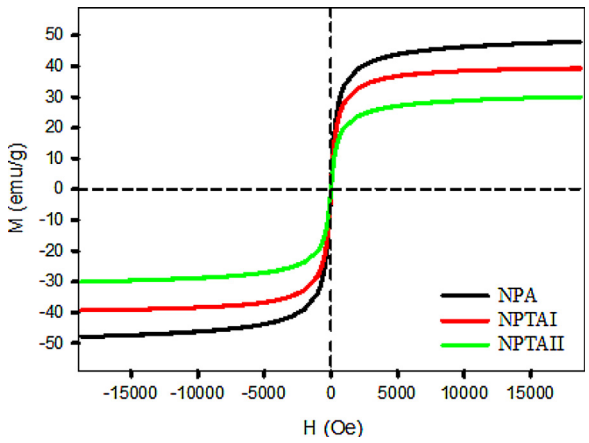

Fig. 4. Magnetization curves for NPA, NPTAI and NPTAII.

nanomaterials with the SBP show the presence of all the signals expected in the presence of an enzyme immobilized at the surface of a material. We have focused our attention on the signals related to amide I and II present in the range 1750–1550 cm^{-1} (Fig. 3) since they allow to obtain insights into the conformation of the immobilized enzyme [28–30]. The spectra have been normalized in order to evidence the intensity ratio of the components, and clearly show that the intensity of the band at around 1650 cm^{-1} decreases in the order NPA-SBP > NPTAI-SBP > NPTAII-SBP. This band arises mainly from the C—O stretching vibration with minor contributions from out-of-phase C—N stretching vibration, C—N deformation and N—H in-plane bending. The extent to which the internal coordinates contribute to the amide I normal mode depends on the backbone structure. That means that the amide I vibration is hardly affected by the nature of the side chain, but depends on the secondary structure of the backbone, therefore this signal is commonly used for the analysis of the secondary structure of a protein [28]. In our spectra, the decrease of the intensity of 1650 cm^{-1} signal can be related to the progressive loss of the α-helix conformation of the supported enzyme with the decrease of the silica amount in the hybrid systems. This result suggests that silica thickness can affect structural conformation of the immobilized SBP.

The ζ-potential values measured from aqueous dispersion of the nanomaterials at pH 7 were 43.2, 26.0 and 38.4 mV for NPA, NPTAI and NPTAII, respectively. Since maghemite and silica coated maghemite nanoparticles present negative ζ-potential at this pH [31,32], the positives potentials observed for the samples suggest the presence of protonated amine groups on the particle's surface, evidencing that the procedure for amino-functionalizing nanomaterials was successful, in agreement with other results. On the other hand, ζ-potential values of −15 mV and −9 mV obtained at pH 7 for aqueous dispersion of NPA-SBP and NPTAII-SBP, respectively, can confirm the immobilization of SBP and support the hypothesis that the amino functional groups at the particle surface are involved in the SBP immobilization.

The N_2 gas-volumetric isotherms of the biocatalyst supports are reported in Fig. S4, in the Supplementary data. All the isotherms are of the type IV, according to IUPAC classification, characteristic of mesoporous materials. Indeed, the hysteresis loops possess different shapes for the samples: they are classified as H2 for MNP and NPA, compatible with ink-bottle pores, and H3 for NPTAI and NPTAII, compatible with slit-shaped pores. These results suggest that APTES and TEOS play different role in the particle coverage and subsequent aggregation: in the former case the presence of APTES does not affect significantly the aggregation of plain nanoparticles, whereas in the latter case, silica produced by TEOS hydrolysis tends to cover and incorporate the nanoparticles giving a complete different network. The results of specific surface area and porosity obtained applying BET and BJH models [33,34] are reported in Table S1. The MNP sample shows a specific surface area of 118 $m^2\ g^{-1}$ and porosity of 0.33 $cm^3\ g^{-1}$ whose size suggests that it is formed by interparticle void space (the particle size never exceed the 20 nm in width). The addition of APTES and TEOS causes the reduction of specific surface area (more important in the case of NPTAII reaching 31 $m^2\ g^{-1}$ of specific surface area and 0.09 $cm^3\ g^{-1}$ of porosity), whereas the aggregation of the particle results less important in the case of NPTAI showing 67 $m^2\ g^{-1}$ of specific surface area and 0.46 $cm^3\ g^{-1}$ of porosity. The addition of SBP does not affect significantly the specific surface area and porosity of supports; therefore the relative data are not reported.

Magnetic characterization was performed by measuring the magnetization hysteresis curves of NPA, NPTAI and NPTAII at room temperature (Fig. 4). All samples exhibited superparamagnetic characteristics, including zero coercivity and remanence. The saturation magnetization (Ms) of the magnetic nanoparticles were 47.9 (NPA), 39.0 (NPTAI), and 30.0 (NPTAII) emu g^{-1}. This trend is correlated with the different TEOS amounts used in the synthesis (i.e., 0, 2.0 and 5.5 mL for NPA, NPTAI and NPTAII, respectively). Thus, the decrease in Ms for all the samples compared to the maghemite (74 emu g^{-1}) [31] is most likely attributed to the presence of inorganic/organic coating agents that decrease the amount of maghemite per gram of sample. Also, some studies suggested that the presence of the coating agents decreases the uniformity due to quenching of surface moments, resulting in the reduction of magnetic moments in such nanoparticles [35]. Although higher amounts of TEOS (thicker silica shell) decrease the Ms values of the nanomaterials, the separation of all the nanomaterials synthesised from their aqueous dispersions can be easily completed in a few minutes with the applications of an external magnetic field.

3.2. MG degradation by the magnetic biocatalysts

Preliminary experiments related to the MG degradation by free SBP were performed. Since the concentration of H_2O_2 significantly influences the enzymatic degradation rates [6], MG degradation experiments were carried out with different H_2O_2 initial concentrations (Fig. S5, in the Supplementary data). The highest enzymatic performance was obtained at initial ratio $[H_2O_2]/[MG] = 10$ (i.e. $[H_2O_2] = 0.8$ mM and $[MG] = 0.08$ mM), therefore the experiments to test the enzymatic activity of the SBP immobilized on the magnetic nanoparticles were performed at $[H_2O_2]_0 = 0.8$ mM.

Fig. 5 shows MG degradation profiles obtained with the magnetic biocatalysts in the presence of H_2O_2. A good efficiency in MG removal was achieved by NPTAI-SBP and NPTAII-SBP (88% and

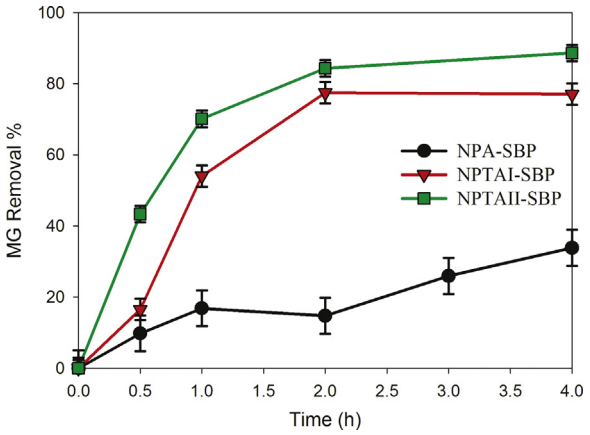

Fig. 5. MG degradation at 28 °C in acetate buffer, pH 5.5, 0.1 M in the presence of different biocatalysts. [biocatalyst] = 2 g L^{-1}; [MG] = 0.08 mM, [H_2O_2] = 0.8 mM. Reactions were performed by triplicate, error bars represents the standard deviations.

Table 2
Activity and activity yields for NPA-SBP, NPTAI-SBP and NPTAII-SBP.

Sample	Activity (μmol (MG) min^{-1} g^{-1} SBP)	Activity yield (%)
NPA-SBP	3.8	4.0
NPTAI-SBP	11.9	12.6
NPTAII-SBP	41.1	43.6
free SBP	94.3	–

77% respectively in 4 h), whereas NPA-SBP reached only a 43% of removal in the same time interval. Peroxidase activities were calculated as the initial MG degradation rate per gram of SBP and the *activity yields* were calculated as the percentage ratio between peroxidase activity of immobilized and free SBP, which represents the efficiency of the heterogeneous biocatalysts with respect to the homogeneous one (Table 2).

Although the amount of enzyme immobilized in each sample increases in the order NPTAII-SBP < NPA-SBP < NPTAI-SBP (Table 1), the activity and activity yield increases following the order NPA-SBP < NPTAI-SBP < NPTAII-SBP, indicating that activity yields are not directly correlated with the amount of immobilized enzyme. On the other hand, immobilization of enzymes usually implies a loss of activity; reported data using aminopropyl glass beads as support showed activity yields of 3% and 35% for horseradish peroxidase and SBP, respectively, after immobilization [13,14]. Analogous loss of activity is observed in the present case, nevertheless, given the recoverability of the enzyme in the magnetic biocatalysts, the activity yield reached by NPTAII-SBP (43.7%) can be considered excellent. There are several possible explanations concerning how SBP loses activity after immobilization procedure. The most probable one concerns the change of the conformation due to intense interactions protein-support affecting the native conformation of the enzyme. Indeed, as previously shown by EPR studies, the covalent immobilization on solid particles induces a partial change in the geometry of the SBP Fe(III)-heme group, that probably affects the catalytic performance [14]. Furthermore, in the present case, iron oxide nanoparticles, being polar and nanometric in size surely exert a strong electric field on neighbouring enzyme molecules, in particular when they are not shielded by the siliceous coating. Actually, HR-TEM images do not evidence the presence of silica in NPA-SBP sample, whereas layers of different of thickness of amorphous silica decorates the crystalline iron oxide particles of samples NPTAI-SBP and NPTAII-SBP respectively. Moreover, the analysis of the changes in the FTIR spectra (Fig. 3) suggested a progressive loss of the α-helix conformation of the supported enzyme with the decrease of the silica amount. It is well established that relatively higher α-helix and lower β-sheet and random coil contents in Horseradish peroxidase favours the enzyme activity [36]. Therefore the evidence can be connected to the corresponding decrease of the biocatalytic activity and consequently the obtained result indicates the way of optimizing the enzymatic activity by tuning the thickness of silica shell around the magnetic support.

Despite the enzymatic-mediated oxidation process, other additional reaction pathways, as HO• radicals–mediated degradation, could be involved in the degradation of MG under the experimental conditions tested. Sun and Lemley [37] demonstrated that magnetite nanoparticles are able to oxidize organic substrates in the presence of H_2O_2 through a heterogeneous Fenton-like process. Also, Lehman et al. [38] showed that silica nanoparticles in combination with H_2O_2 are able to generate small amount of HO•. To better understand the mechanism followed by our systems, MG degradation experiments were performed in the presence of 2-propanol or methanol, two well-known HO• radicals scavengers [39]. Results showed no relevant inhibition of the biocatalysts performance for both free and supported-SBP (Table S1, Supplementary data), indicating that although HO• radicals could be generated by the reaction pathways mentioned above, the HO• radical-mediated MG oxidation can be ruled out in our experimental conditions. On the other hand, control experiments in the absence of H_2O_2, showed no changes in the dye concentrations during the experiments, therefore we can exclude the removal of the substrate given by non-oxidative pathways (e.g. adsorption).

The effect of the temperature on the activity of the supported peroxidase was further investigated (Fig. 6A). Different trends were observed for the three magnetic biocatalysts. NPA-SBP evidenced a slight increase of the activity with temperature but, in the temperature range studied, the activity was much lower than those of NPTAI-SBP and NPTAII-SBP. Otherwise, NPTAI-SBP and NPTAII-SBP show a clear increase of activity reaching a maximum at 50–60 °C (for NPTAI-SBP) and 60 °C (for NPTAII-SBP). At higher temperatures the activity of the biocatalysts decreases, but all systems remain active at a temperature as high as 95 °C, as expected for systems containing enzymes thermally stabilised by immobilisation on solid supports [19]. In both these samples the maximum activity is reached at temperatures lower than those previously reported for a crude extract of SBP (80 °C) [2] indicating that the presence of other proteins can play an important role in the activity preservation at high temperatures. Nevertheless, similar results were reported by Horst et al. [19] when catalase is immobilized onto magnetite. It is worth mentioning, that the activity of NPTAII-SBP at 60 °C increases four times with respect to 25 °C, which is higher than the increase reported for free SBP [2]. At temperatures higher than 60 °C also a spontaneous thermal decomposition of H_2O_2 occurs (data not shown), leading to MG oxidation. This process could be responsible for the slight MG degradation increase observed in the NPA-SBP system. However, this contribution is negligible compared with the enzymatic activity observed for NPTAI-SBP and NPTAII-SBP. The trend observed with temperature confirms that the conformation of the enzyme is affected by the strong electric field produced by the iron oxide particle core. In fact, the temperature increase probably allows a thermally-favoured rearrangement of the tertiary structure of the protein which, consequently, becomes more active in MG abatement. This phenomenon is achievable for NPTAI-SBP and, even more, for NPTAII-SBP, whereas it is very limited in the case of NPA-SBP sample, in which the conformational modifications undergone by the protein during the immobilization process are much more pronounced.

The reusability of the catalyst is an important feature for the application in industry or for environmental purposes. The results

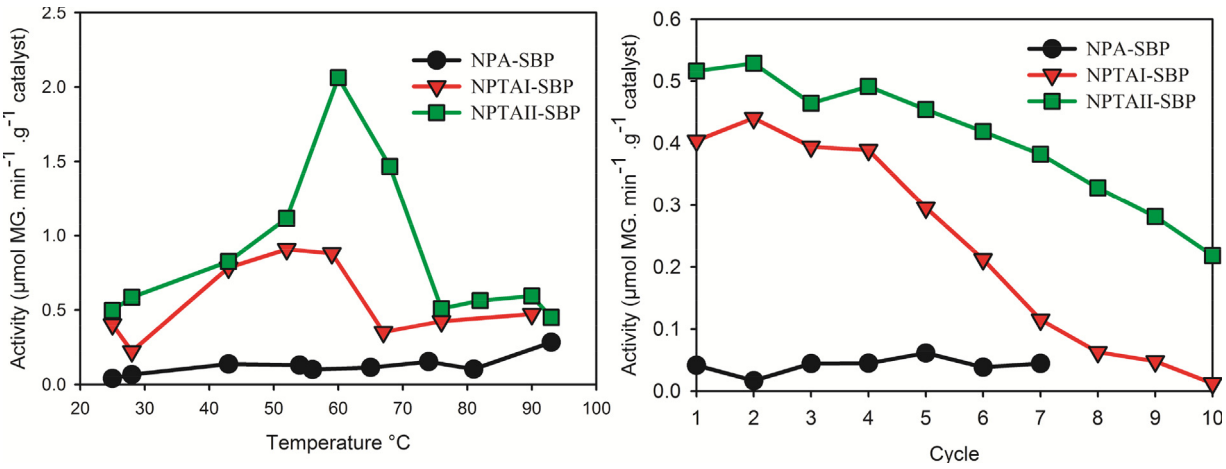

Fig. 6. A) Temperature effect on peroxidase activity for NPA-SBP, NPTAI-SBP and NPTAII-SBP. B) Reuse performance of NPA-SBP, NPTAI-SBP and NPTAII-SBP after each cycle for ten cycles. $[MG]_0$ = 0.0811 mM, $[H_2O_2]_0$ = 0.811 mM, buffer acetate 0.1 M, pH = 5.5.

of the experiments carried out in ten cycles are shown in Fig. 6B. NPTAI-SBP and NPTAII-SBP can be reused for four cycles without significant loss of their initial activity. Furthermore, NPTAII-SBP retains 42% of its initial activity after ten cycles (with a progressive and almost linear loss corresponding to 6.4% per cycle), while NPTAI-SBP retains only 3% of its initial activity after 10 cycles (with a corresponding loss of about 10.8% per cycle starting from the fifth one). The enzymatic activity loss is commonly attributed to i) the accumulation of the polymeric products at the catalyst surface hindering the access of the substrate to the enzyme active site, ii) enzyme leaching from the support, and iii) the free radical-induced enzyme inactivation [7,10,13]. In our system, the absence of SBP in the analyzed solutions after each cycle, confirm that SBP leaching from the supports can be discarded. It is worth to mention that the ability of the developed materials, in particular NPTAII, in retaining their catalytic activities is enhanced in comparison with previously reported systems, which is encouraging for its application. For example, Galárraga et al. [40] obtained a 40% of activity loss after only four cycles with SBP immobilized on corncob powder, whereas Prokopijevic et al. [12] obtained a 78% of loss at the sixth cycle with macroporous glycidyl methacrylates as support.

4. Conclusions

In this study, a facile and effective method of immobilization of SBP onto magnetic nanoparticles modified with TEOS and APTES is described. Different amounts of TEOS in the synthesis procedure were investigated and a deep physicochemical characterization of such materials was performed. Magnetic iron oxide nanoparticles of 10 nm diameter with different silica shell thickness externally modified with amino groups were synthesized as biocatalyst supports. Results showed that the increase of TEOS amount causes the decrease in the specific surface area and saturation magnetization of the supported biocatalyst, but favours a higher retention of the α-helix conformation in the immobilized SBP. The enzymatic activities of immobilized SBP in different conditions were tested using Malachite Green. The silica shell coating the iron-based nanoparticles seems to play a key role in preserving the enzymatic activity of SBP in terms of materials reusability and thermostability. The encouraging results display a great potential for the use of immobilized SBP in wastewater treatment and may pave the way towards hybrid biocatalysts where the structural conformation of the enzyme can be optimised in order to reach the free enzyme activity also in heterogeneous systems.

Acknowledgements

Authors acknowledge the economic support of European Union for the project Mat4Treat (H2020-MSCA-RISE-2014, Project 645551), Compagnia di San Paolo and Torino University for the project Microbusters (Torino_call2014_L2_126 "Bando per il finanziamento di progetti di ricerca di ateneo – anno 2014"), UNLP (11/X679) and CONICET (PIP: 12–2013-01-00236CO). A. Donadelli thanks CONICET for his research graduate grant. L. Carlos and F. S. García Einschlag are research members of CONICET.

Appendix A. Supplementary data

Supplementary data associated with this article can be found, in the online version, at https://doi.org/10.1016/j.colsurfb.2017.11.043.

References

[1] E. Torres, I. Bustos-Jaimes, S. Le Borgne, Appl. Catal. B Environ. 46 (2003) 1–15.
[2] Z. Geng, K. Jagannadha Rao, A.S. Bassi, M. Gijzen, N. Krishnamoorthy, Catal. Today 64 (2001) 233–238.
[3] A. Steevensz, S. Madur, W. Feng, K.E. Taylor, J.K. Bewtra, N. Biswas, Enzyme Microb. Technol. 55 (2014) 65–71.
[4] B. Boscolo, E. Laurenti, E. Ghibaudi, Protein J. 25 (2006) 379–390.
[5] A. Henriksen, O. Mirza, C. Indiani, K. Teilum, G. Smulevich, K.G. Welinder, M. Gajhede, Protein Sci. 10 (2001) 108–115.
[6] Y.J. Choi, H.J. Chae, E.Y. Kim, J. Biosci. Bioeng. 88 (1999) 368–373.
[7] M.C. Silva, J.A. Torres, F.G.E. Nogueira, T.S. Tavares, A.D. Corrêa, L.C.A. Oliveira, T.C. Ramalho, RSC Adv. 6 (2016) 83856–83863.
[8] C. Ispas, I. Sokolov, S. Andreescu, Anal. Bioanal. Chem. 393 (2009) 543–554.
[9] E. Ranjbakhsh, A.K. Bordbar, M. Abbasi, A.R. Khosropour, E. Shams, Chem. Eng. J. 179 (2012) 272–276.
[10] S.C. Corgié, P. Kahawong, X. Duan, D. Bowser, J.B. Edward, L.P. Walker, E.P. Giannelis, Adv. Funct. Mater. 22 (2012) 1940–1951.
[11] K. Can, M. Ozmen, M. Ersoz, Colloids Surf. B 71 (2009) 154–159.
[12] M. Prokopijevic, O. Prodanovic, D. Spasojevic, Z. Stojanovic, K. Radotic, R. Prodanovic, Bioprocess Biosyst. Eng. 37 (2014) 799–804.
[13] Y.C. Lai, S.C. Lin, Process Biochem. 40 (2005) 1167–1174.
[14] T. Marchis, G. Cerrato, G. Magnacca, V. Crocellà, E. Laurenti, Biochem. Eng. J. 67 (2012) 28–34.
[15] P. Calza, P. Avetta, G. Rubulotta, M. Sangermano, E. Laurenti, Chem. Eng. J. 239 (2014) 87–92.
[16] L.M. Rossi, N.J.S. Costa, F.P. Silva, R. Wojcieszak, Green Chem. 16 (2014) 2906.
[17] H. Vaghari, M. Jafarizadeh-Malmiri, A. Mohammadlou, N. Berenjian, N. Anarjan, S. Jafari, Biotechnol. Lett. 38 (2016) 223–233.
[18] D. Maity, D.C. Agrawal, J. Magn. Magn. Mater. 308 (2007) 46–55.
[19] F. Horst, E.H. Rueda, M.L. Ferreira, Enzyme Microb. Technol. 38 (2006) 1005–1012.
[20] S.A. Mohamed, M.H. Al-Harbi, Y.Q. Almulaiky, I.H. Ibrahim, R.M. El-Shishtawy, Electron. J. Biotechnol. 27 (2017) 84–90.
[21] R.P. Pogorilyi, I.V. Melnyk, Y.L. Zub, G.A. Seisenbaeva, V.G. Kessler, Colloids Surf. B 144 (2016) 135–142.

[22] S.J. Culp, F.A. Beland, J. Am. Coll. Toxicol. 15 (1996) 219–238.
[23] K. Gupta, O.P. Khatri, J. Colloid Interface Sci. 501 (2017) 11–21.
[24] J.K.A. Kamal, D.V. Behere, J. Inorg. Biochem. 94 (2003) 236–242.
[25] S. Saidman, E.H. Rueda, M.L. Ferreira, Biochem. Eng. J. 28 (2006) 177–186.
[26] S. Alibeigi, M.R. Vaezi, Chem. Eng. Technol. 31 (2008) 1591–1596.
[27] K.L. de Almeida, P.P.C. Caiado, D.O. Sartoratto, A.R. Cintra e Silva, P.C. Pereira, J. Alloys Compd 500 (2010) 149–152.
[28] A. Barth, Biochim. Biophys. Acta Bioenerg. 2007 (1767) 1073–1101.
[29] C. Jung, Anal. Bioanal. Chem. 392 (2008) 1031–1058.
[30] S.E. Rodríguez-deLuna, I.E. Moreno-Cortez, M.A. Garza-Navarro, R. Lucio-Porto, L. López Pavón, V.A. González-González, J. Appl. Polym. Sci. 134 (2017) 44811.
[31] C.J. Serna, M.P. Morales, in: M. Matijevic, E. Borkovec (Eds.), Surf. Colloid Sci., Springer, US, 2004, pp. 27–81.
[32] V. Maurice, T. Georgelin, J.M. Siaugue, V. Cabuil, J. Magn. Magn. Mater. 321 (2009) 1408–1413.
[33] S. Brunauer, P.H. Emmett, E. Teller, J. Am. Chem. Soc. 60 (1938) 309–319.
[34] E.P. Barrett, L.G. Joyner, P.P. Halenda, J. Am. Chem. Soc. 73 (1951) 373–380.
[35] D.K. Kim, M. Mikhaylova, Y. Zhang, M. Muhammed, M. Mikhaylova, Y. Zhang, M. Muhammed, Chem. Mater 15 (2003) 1617–1627.
[36] B.-P. Wu, Q. Wen, H. Xu, Z. Yang, J. Mol. Catal. B Enzym. 101 (2014) 101–107.
[37] A.T. Sun, J. Mol. Catal. A Chem. 349 (2011) 71–79.
[38] S.E. Lehman, A.S. Morris, P.S. Mueller, A.K. Salem, V.H. Grassian, S.C. Larsen, Environ. Sci. Nano (2015).
[39] S. Gligorovski, R. Strekowski, S. Barbati, D. Vione, Chem. Rev. 115 (2015) 13051–13092.
[40] J. César, V. Galárraga, A. Francisco, J.C. Bassan, A.J. Goulart, Rev. Ciénc. Farm. Básica Apl. 34 (2013) 321–326.